

Proximal Residual Flows for Bayesian Inverse Problems

Johannes Hertrich*

December 1, 2022

Normalizing flows are a powerful tool for generative modelling, density estimation and posterior reconstruction in Bayesian inverse problems. In this paper, we introduce proximal residual flows, a new architecture of normalizing flows. Based on the fact, that proximal neural networks are by definition averaged operators, we ensure invertibility of certain residual blocks. Moreover, we extend the architecture to conditional proximal residual flows for posterior reconstruction within Bayesian inverse problems. We demonstrate the performance of proximal residual flows on numerical examples.

1 Introduction

Generative models for approximating complicated and high-dimensional probability distributions gained increasingly attention over the last years. One subclass of generative models are normalizing flows [13, 43]. They are learned diffeomorphisms which push forward a complicated probability distribution to a simple one. More precisely, we learn a diffeomorphism \mathcal{T} such that a distribution P_X can be approximately represented as $\mathcal{T}_{\#}^{-1}P_Z$ for a simple distribution P_Z . Several architectures of normalizing flows were proposed in the literature including Glow [34], real NVP [14], continuous normalizing flows [7, 18, 39] and autoregressive flows [11, 15, 31, 40]. In this paper, we particularly focus on residual flows [4, 8]. Here, the basic idea is that residual neural networks [23] are invertible as long as each subnetwork has a Lipschitz constant smaller than one. In [30], the authors figure out a relation between residual flows and Monge maps in optimal transport problems. For training residual flows, one needs to control the Lipschitz constant of the considered subnetworks. Training neural networks with a prescribed Lipschitz constant was addressed

*Institute of Mathematics, TU Berlin, Straße des 17. Juni 136, D-10623 Berlin, Germany, j.hertrich@math.tu-berlin.de

in several papers [17, 37, 41, 45]. For example, the authors of [37] propose to rescale the transition matrices after each optimization step such that the spectral norm is smaller or equal than one. However, it is well known that enforcing a small Lipschitz constant within a neural network can lead to limited expressiveness.

In this paper, we propose to overcome these limitations by using proximal neural networks (PNNs). PNNs were introduced in [22, 26] and are by construction averaged operators. Using scaled PNNs as subnetworks, we prove that a residual neural network is invertible even if the scaled PNN has a Lipschitz constant larger than one. Further, we consider Bayesian inverse problems

$$Y = F(X) + \eta,$$

with an ill-posed forward operator F and some noise η . Here, we aim to reconstruct the posterior distributions $P_{X|Y=y}$ with using normalizing flows. To this end, we apply a conditional generative model [3, 20, 36, 46]. For normalizing flows, this means that we aim to learn a mapping $\mathcal{T}(y, x)$ such that for any y it holds approximately $P_{X|Y=y} \approx \mathcal{T}(y, \cdot)_{\#}^{-1} P_Z$ for a simple distribution P_Z . Further, we show how proximal residual flows can be used for conditional generative modeling by constructing conditional proximal residual flows. Finally, we demonstrate the power of (conditional) proximal residual flows by numerical examples. First, we use proximal residual flows for sampling and density estimation of some complicated probability distributions including adversarial toy examples and molecular structures. Afterwards, we apply conditional proximal residual flows for reconstructing the posterior distribution in an inverse problem of scatterometry and for certain mixture models.

The paper is organized as follows. In Section 2, we first revisit residual flows and proximal neural networks. Afterwards we introduce proximal residual flows which combine both. Then, we extend proximal residual flows to Bayesian inverse problems in Section 3. We demonstrate the performance of proximal residual flows in Section 4. Conclusions are drawn in Section 5.

2 Proximal Residual Flows

Given i.i.d. samples x_1, \dots, x_N from an n -dimensional random variable X with unknown distribution P_X , a normalizing flow aims to learn a diffeomorphism $\mathcal{T}: \mathbb{R}^n \rightarrow \mathbb{R}^n$ such that $P_X \approx \mathcal{T}_{\#}^{-1} P_Z$. To this end, the diffeomorphism will be a neural network \mathcal{T}_{θ} with parameters θ , which is by construction invertible. For the training, we consider the maximum likelihood loss, i.e., we minimize

$$\mathcal{L}(\theta) = \sum_{i=1}^N p_{\mathcal{T}_{\theta\#}^{-1} P_Z}(x_i).$$

Note, that using the change of variables formula for probability density functions, we have that $p_{\mathcal{T}_\theta^{-1}P_Z}(x)$ can be computed by

$$p_{\mathcal{T}_\theta^{-1}P_Z}(x) = p_Z(\mathcal{T}_\theta(x))|\nabla\mathcal{T}_\theta(x)|.$$

In this section, we propose a new architecture for normalizing flows based on residual flows [8] and proximal neural networks [22, 26].

2.1 Residual Flows

Residual flows were introduced in [4, 8]. The basic idea is to consider residual neural networks, where each subnetwork is constraint to be c -Lipschitz continuous for some $c < 1$, i.e., we have $T = L_K \circ \dots \circ L_1$, where each mapping L_k has the form

$$L: \mathbb{R}^n \rightarrow \mathbb{R}^n, \quad L(x) = x + g(x), \quad \text{Lip}(g) < 1.$$

Then, Banach's fix point theorem yields that L is invertible and the inverse $L^{-1}(y)$ can be computed by the limit of the iteration

$$x^{(r+1)} = y - g(x^{(r)}), \quad x^{(0)} = y.$$

For ensuring the Lipschitz continuity of g during the training of residual flows, the authors of [4, 8] suggested to use spectral normalization [17, 37]. Finally, to evaluate and differentiate $\log(|\nabla\mathcal{T}(x)|)$, we have to evaluate and differentiate $\log(|\nabla L(x)|)$ for each residual block L . In small dimensions, this can be done by algorithmic differentiation, which is in high dimensions computationally intractable. Here we can apply the following theorem is from [8, Theorem 1, Theorem 2] which is based on an expansion of ∇L into a Neumann series.

Theorem 1. *Let Q be a random variable on $\mathbb{Z}_{>0}$ such that $P(Q = k) > 0$ for all $k \in \mathbb{Z}_{>0}$ and define $p_k = P(Q \geq k)$. Consider the function $L(x) = x + g(x)$, where $g: \mathbb{R}^n \rightarrow \mathbb{R}^n$ is differentiable and fulfills $\text{Lip}(g) < 1$. Then, it holds*

$$\log(|\nabla L(x)|) = \mathbb{E}_{v \sim \mathcal{N}(0, I), q \sim P_Q} \left[\sum_{k=1}^q \frac{(-1)^{k+1}}{k} \frac{v^\top (\nabla g(x))^k v}{p_k} \right]$$

and

$$\frac{\partial}{\partial \theta} \log(|\nabla L(x)|) = \mathbb{E}_{v \sim \mathcal{N}(0, I), q \sim P_Q} \left[\left(\sum_{k=0}^q \frac{(-1)^k}{p_k} v^\top (\nabla g(x))^k \right) \frac{\partial (\nabla g(x))}{\partial \theta} v \right].$$

2.2 Proximal Neural Networks

Averaged operators and in particular proximity operators received increasingly attention in deep learning over the last years [6, 9, 16]. For a proper, convex and lower semi-continuous function $f: \mathbb{R}^d \rightarrow \mathbb{R} \cup \{\infty\}$, the proximity operator of f is given by

$$\text{prox}_{\lambda f}(x) = \arg \min_{y \in \mathbb{R}^n} \left\{ \frac{1}{2\lambda} \|x - y\|^2 + f(y) \right\}.$$

Proximity operators are in particular $\frac{1}{2}$ -averaged operators, i.e.,

$$\text{prox}_{\lambda f}(x) = \frac{1}{2}x + \frac{1}{2}R(x), \quad \text{for some } R \text{ with } \text{Lip}(R) \leq 1.$$

In [10] the authors observed that most activation functions of neural networks are proximity operators. They proved that an activation function σ is a proximity operator with respect to some function g , which has 0 as a minimizer, if and only if σ is 1-Lipschitz continuous, monotone increasing and fulfills $\sigma(0) = 0$. They called the class of such activation functions *stable activation functions*. Using this result, Proximal Neural Networks (PNNs) were introduced in [22] as the concatenation of blocks of the form

$$B(\cdot; T, b, \alpha) := T^T \sigma_\alpha(T \cdot + b),$$

where $b \in \mathbb{R}^d$, T or T^T is in the Stiefel manifold $\text{St}(n, m) = \{T \in \mathbb{R}^{n, m} : T^T T = I\}$ and σ_α is a stable activation function which may depend on some additional parameter α . It can be shown that B is again a proximity operator of some proper, convex and lower semi-continuous function, see [22]. Now a PNN with K layers is defined as

$$\Phi(\cdot; u) = B_K(\cdot; T_K, b_K, \alpha_K) \circ \cdots \circ B_1(\cdot; T_1, b_1, \alpha_1),$$

where $u = ((T_k)_{k=1}^K, (b_k)_{k=1}^K, (\alpha_k)_{k=1}^K)$. Since Φ is the concatenation of K $\frac{1}{2}$ -averaged operators, we obtain that Φ is $K/(K+1)$ -averaged. From a numerical viewpoint, it was shown in [26] that (scaled) PNNs show a comparable performance as usual convolutional neural networks for denoising.

The training of PNNs is not straightforward due to the condition that T or T^T are contained in the Stiefel manifold. The authors of [22, 26, 27] propose a stochastic gradient descent on the manifold of the parameters, the minimization of a penalized functional and a stochastic variant of the inertial PALM algorithm [5, 42]. However, to ensure the invertibility of proximal residual flows, it is important that the constraint $T_k \in \text{St}(n, m)$ is fulfilled during the full training procedure. Therefore, we propose the following different training procedure.

Instead of training the matrices T_k directly, we define $T_k = P_{\text{St}(n, m)}(\tilde{T}_k)$, where $P_{\text{St}(n, m)}$ denotes the orthogonal projection onto the Stiefel manifold. For dense matrices and convolutions with full filter length, this projection is given by the U -factor of the polar decomposition, see [29, Sec. 7.3, Sec. 7.4], and can be computed by the iteration

$$Y_{n+1} = 2Y_n(I + Y_n^T Y_n)^{-1}, \quad Y_0 = \tilde{T}_k.$$

see [28, Chap. 8]. Unfortunately, we are not aware of a similar iterative algorithm for convolutions with limited filter length. Finally, we optimize the matrices \tilde{T}_k instead of the matrices T_k . In order to ensure numerical stability, we regularize the distance of \tilde{T}_k to the Stiefel manifold by the penalizer $\|\tilde{T}_k^T \tilde{T}_k - I\|_F^2$.

2.3 Proximal Residual Flows

Now, we propose proximal residual flows as the concatenation $T = L_K \circ \dots \circ L_1$ of residual blocks L_k of the form

$$L_k(x) = x + \gamma_k \Phi_k(x), \quad (1)$$

where $\gamma_k > 0$ is some constant and Φ_k is a PNN. The following proposition ensures the invertibility of L_k and T .

Proposition 2. *Let Φ be a t -averaged operator with $\frac{1}{2} < t \leq 1$ and let $0 < \gamma < \frac{1}{2t-1}$. Then, the function $L(x) = x + \gamma\Phi(x)$ is invertible and the inverse $L^{-1}(y)$ is given by the limit of the sequence*

$$x^{(r+1)} = \frac{1}{1 + \gamma - \gamma t} y - \frac{\gamma t}{1 + \gamma - \gamma t} R(x^{(r)}), \quad \text{where } R(x) := \frac{1}{t} \Phi(x) - \frac{1-t}{t} x.$$

Additionally, if Φ is t -averaged with $0 \leq t \leq \frac{1}{2}$, then the above statement is true for arbitrary $\gamma > 0$.

Note that $t = 1$ in the proposition exactly recovers the case considered in [4].

Proof. Since Φ is t -averaged, we get $\Phi = (1-t)I + tR$, where $R := \frac{1}{t}\Phi - \frac{1-t}{t}I$ is 1-Lipschitz continuous. Further, note that $\gamma < \frac{1}{2t-1}$ is equivalent to $\frac{\gamma t}{1+\gamma-\gamma t} < 1$. Therefore, Banach's fix point theorem yields that the sequence $(x^{(r)})_r$ converges to the unique fix point x of

$$x = \frac{1}{1 + \gamma - \gamma t} y - \frac{\gamma t}{1 + \gamma - \gamma t} R(x)$$

which is equivalent to $y = x + \frac{\gamma}{2}(I + R)(x) = x + \gamma\Phi$. In particular, x is the unique solution of $L(x) = y$. In the case $t \leq \frac{1}{2}$, we have that $\frac{\gamma t}{1+\gamma-\gamma t} < 1$ is true for any $\gamma > 0$ such that the same argumentation applies. \square

Using the proposition, we obtain, that L_k from (1) is invertible, as long as $0 < \gamma_k < \frac{\kappa+1}{\kappa-1}$, where κ is the number of layers of Φ_k . In contrast to residual flows, the subnetworks $\gamma_k \Phi_k$ of proximal residual flows may have Lipschitz constants larger than 1. For instance, if $\kappa = 3$, then the upper bound on the Lipschitz constant of the subnetwork is 2 instead of 1.

Remark 3. *Let $\Phi = B_K \circ \dots \circ B_1: \mathbb{R}^n \rightarrow \mathbb{R}^n$ be a PNN with layers $B_i(x) = T_i^T \sigma(T_i x + b_i)$. Then, by definition, it holds $B_k \circ \dots \circ B_1(x) \in \mathbb{R}^n$ for all $k = 1, \dots, K$. In particular,*

each layer of the PNN has at most n neurons, which possibly limits the expressiveness. We overcome this issue with a small trick. Let

$$A = \frac{1}{\sqrt{p}} \begin{pmatrix} I \\ \vdots \\ I \end{pmatrix} \in \text{St}(pn, n)$$

and let $\Phi: \mathbb{R}^{pn} \rightarrow \mathbb{R}^{pn}$ be t -averaged. Then, a simple computation yields that also $\Psi = A^T \Phi(A \cdot)$ is a t -averaged operator. In particular, we can use a PNN with pn neurons in each layer instead of a PNN with n neurons in each layer, which increases the expressiveness of the network a lot.

For the evaluation of $\log(|\nabla \mathcal{T}(x)|)$, we adapt Theorem 1 for proximal residual flows.

Corollary 4. *Let Q be a random variable on $\mathbb{Z}_{>0}$ such that $P(Q = k) > 0$ for all $k \in \mathbb{Z}_{>0}$ and define $p_k = P(Q \geq k)$. Consider the function $L(x) = x + \gamma \Phi(x)$, where $\Phi: \mathbb{R}^n \rightarrow \mathbb{R}^n$ is differentiable and t -averaged for $t \in (\frac{1}{2}, 1]$ and $0 < \gamma < \frac{1}{2t-1}$. Then, it holds*

$$\log(|\nabla L(x)|) = \mathbb{E}_{v \sim \mathcal{N}(0, I), q \sim P_Q} \left[\sum_{k=1}^q \frac{(-1)^{k+1}}{k} \frac{v^T (\frac{\gamma t}{1+\gamma-\gamma t} \nabla R(x))^k v}{p_k} \right] + n \log(1 + \gamma - \gamma t),$$

where $R(x) = \frac{1}{t} \Phi(x) - \frac{1-t}{t} x$. Further, we have

$$\frac{\partial}{\partial \theta} \log(|\nabla L(x)|) = \mathbb{E}_{v \sim \mathcal{N}(0, I), q \sim P_Q} \left[\left(\sum_{k=0}^q \frac{(-1)^k}{p_k} v^T (\frac{\gamma t}{1+\gamma-\gamma t} \nabla R(x))^k \right) \frac{\partial (\frac{\gamma t}{1+\gamma-\gamma t} \nabla R(x))}{\partial \theta} v \right].$$

Additionally, if Φ is t -averaged for $0 \leq t \leq \frac{1}{2}$, then the above statement holds true for any $\gamma > 0$.

Proof. Since Φ is t -averaged, it holds $\Phi = (1-t)I + tR$, where $R = \frac{1}{t}\Phi - \frac{1-t}{t}I$ is 1-Lipschitz continuous. Thus, we have

$$L = (1 + \gamma - \gamma t)I + \gamma t R = (1 + \gamma - \gamma t) \left(I + \frac{\gamma t}{1+\gamma-\gamma t} R \right),$$

such that

$$\log(|\nabla L(x)|) = \log(|\nabla (I + \frac{\gamma t}{1+\gamma-\gamma t} R)(x)|) + n \log(1 + \gamma - \gamma t).$$

Now, since $\frac{\gamma t}{1+\gamma-\gamma t} < 1$, applying Theorem 1 with $g = \frac{\gamma t}{1+\gamma-\gamma t} R$ gives the assertion. \square

In the special case, that the PNN Φ consists of only one layer, we can derive the log-determinant explicitly by the following lemma.

Lemma 5. Let $\Phi(x) = T^T \sigma(Tx + b)$ for $T^T \in \text{St}(n, m)$, $n \geq m$ and a differentiable activation function $\sigma: \mathbb{R} \rightarrow \mathbb{R}$. Then, the log-determinant of the Jacobian of $L(x) = x + \gamma\Phi(x)$ is given by

$$\log(|\nabla L(x)|) = \sum_{i=1}^m \log(1 + \gamma\sigma'_i(Tx + b)),$$

where $\sigma'_i(Tx + b)$ is the i th component of $\sigma'(Tx + b)$.

Proof. Let \tilde{T} be a matrix, such that $S = (T^T|\tilde{T}^T) \in \mathbb{R}^{n \times n}$ is an orthogonal matrix. We have that

$$\nabla\Phi(x) = T^T \sigma'(Tx + b)T, \quad \nabla L(x) = I_n + \gamma T^T \sigma'(Tx + b)T.$$

Then, by orthogonality of S , it follows

$$|\nabla L(x)| = |S^T| |I_n + \gamma T^T \sigma'(Tx + b)T| |S| = |I_n + \gamma(TS)^T \sigma'(Tx + b)(TS)|.$$

Since $T^T \in \text{St}(n, m)$, it holds by the definition of S that $TS = (I_m|0)$ such that

$$|\nabla L(x)| = \left| \begin{pmatrix} I_m + \gamma\sigma'(Tx + b) & 0 \\ 0 & I_{n-m} \end{pmatrix} \right| = \prod_{i=1}^m 1 + \gamma\sigma'_i(Tx + b).$$

Taking the logarithm proves the statement. \square

3 Conditional Proximal Residual Flows

In the following, we consider for a random variable X the inverse problem

$$Y = F(X) + \eta, \tag{2}$$

where $F: \mathbb{R}^n \rightarrow \mathbb{R}^d$ is an ill-posed/ill-conditioned forward operator and η is some noise. Now, we aim to train a conditional normalizing flow model for reconstructing all posterior distributions $P_{X|Y=y}$, $y \in \mathbb{R}^d$. More precisely, we want to learn a mapping $\mathcal{T}: \mathbb{R}^d \times \mathbb{R}^n \rightarrow \mathbb{R}^n$ such that $\mathcal{T}(y, \cdot)$ is invertible for all $y \in \mathbb{R}^d$ and

$$P_{X|Y=y} = \mathcal{T}(y, \cdot)_{\#}^{-1} P_Z.$$

For this purpose, \mathcal{T}_θ will be a neural network with parameters θ . We learn \mathcal{T}_θ from i.i.d. samples $(x_1, y_1), \dots, (x_N, y_N)$ of (X, Y) using the maximum likelihood loss

$$\mathcal{L}(\theta) = \sum_{i=1}^N p_{\mathcal{T}_\theta(y_i, \cdot)_{\#}^{-1} P_Z}(x_i) \approx \mathbb{E}_{y \sim P_Y} [\text{KL}(P_{X|Y=y}, P_{\mathcal{T}_\theta(y, \cdot)_{\#}^{-1} P_Z})] + \text{const.}$$

Note that for the real NVP architecture [14], such flows were considered in [3, 12, 20].

For using proximal residual flows as conditional normalizing flows, we need the following lemma.

Lemma 6. Let $\Phi = (\Phi_1, \Phi_2): \mathbb{R}^d \times \mathbb{R}^n \rightarrow \mathbb{R}^d \times \mathbb{R}^n$ be a t -averaged operator. Then, for any $y \in \mathbb{R}^d$, the operator $\Phi_2(y, \cdot)$ is t -averaged.

Proof. Since Φ is t -averaged, we have that $\Phi(y, x) = (1 - t)(y, x) + tR(y, x)$ for some 1-Lipschitz function $R = (R_1, R_2): \mathbb{R}^n \times \mathbb{R}^d \rightarrow \mathbb{R}^n \times \mathbb{R}^d$. Now let $y \in \mathbb{R}^d$ be arbitrary fixed. Due to the Lipschitz continuity of R , it holds for $x_1, x_2 \in \mathbb{R}^n$ that

$$\|R(y, x_1) - R(y, x_2)\| \leq \|(y, x_1) - (y, x_2)\| = \|x_1 - x_2\|.$$

Thus, $R_2(\cdot, y)$ is 1-Lipschitz continuous and we get by definition that

$$\Phi_2(y, x) = (1 - t)x + tR_2(y, x),$$

such that $\Phi_2(y, \cdot)$ is a t -averaged operator. \square

Now, we define a conditional proximal residual flows as a mapping $\mathcal{T}: \mathbb{R}^d \times \mathbb{R}^n \rightarrow \mathbb{R}^n$ given by $\mathcal{T}(\cdot, y) = L_K(\cdot, y) \circ \dots \circ L_1(\cdot, y)$ with

$$L_k(y, x) = x + \gamma_k \Phi_{k,2}(y, x), \quad (3)$$

where $\Phi_k = (\Phi_{k,1}, \Phi_{k,2}): \mathbb{R}^n \times \mathbb{R}^d \rightarrow \mathbb{R}^n \times \mathbb{R}^d$ is a PNN. By definition, we have that $\mathcal{T}(y, \cdot)$ is a proximal residual flow for any fixed y such that the invertibility result in Proposition 2 applies.

4 Numerical Examples

In this section, we demonstrate the performance of proximal residual flows by numerical examples. First, in Subsection 4.1 we apply proximal residual flows in an unconditional setting. Afterwards, in Subsection 4.2, we consider a conditional setting with Bayesian inverse problems. In both cases, we compare our results with residual flows [4, 8] and a variant of the real NVP architecture [2, 14]. Within all architectures we use activation normalization [34] after every invertible block. For evaluating the quality of our results, we will use the following error measures.

- The **empirical Kullback Leibler divergence** of two probability measures P and Q on $[0, 1]^d$ approximates $\text{KL}(P, Q)$ based on samples. Given samples x_1, \dots, x_N of P and samples y_1, \dots, y_M of Q , the empirical KL divergence of P and Q on $[0, 1]^d$ using a $d_1 \times \dots \times d_d$ grid is given by

$$\sum_{i_1=0}^{d_1-1} \dots \sum_{i_d=0}^{d_d-1} h_{i_1, \dots, i_d} \log \left(\frac{h_{i_1, \dots, i_d}}{\tilde{h}_{i_1, \dots, i_d}} \right),$$

Method	n	d	K	p	h	γ	b	e	s	τ
Toy examples	2	-	20	64	64	1.99	200	20	2000	10^{-3}
Alanine Dipeptide	66	-	20	2	100	1.99	200	20	2000	10^{-3}
Circle	2	1	20	64	64	1.99	800	20	2000	10^{-3}
Scatterometry	3	23	20	10	128	1.99	1600	20	2000	$5 \cdot 10^{-3}$
Mixture models	50	50	20	2	128	1.99	200	20	2000	$5 \cdot 10^{-3}$

Table 1: Implementation details for the numerical experiments. The table contains for each experiment the dimension n , the dimension d of the condition, the number of residual blocks K , the parameter p from Remark 3, the hidden dimension h within the subnetwork, the parameter γ in the equations (1) and (3), the batch size b , the number of epochs e , the number of steps per epoch s and the learning rate τ .

where h and \tilde{h} are the normalized histograms of $(x_i)_i$ and $(y_i)_i$, i.e., h is defined by

$$h_{i_1, \dots, i_d} = \frac{\#\{i : x_i \in [\frac{i_1}{d_1}, \frac{i_1+1}{d_1}] \times \dots \times [\frac{i_d}{d_d}, \frac{i_d+1}{d_d}]\}}{N}$$

and \tilde{h} is defined analogously.

- We evaluate the **empirical Wasserstein distance** of two probability measures P and Q by computing $W_2(\frac{1}{N} \sum_{i=1}^N \delta_{x_i}, \frac{1}{N} \sum_{i=1}^N \delta_{y_i})$, where the x_i are iid samples from P and the y_i are iid samples from Q .

All implementations are done in Python and Tensorflow. We run them on a single NVIDIA GeForce GTX 2060 Super GPU with 8 GB memory. For the training we use the Adam optimizer [33]. The training parameters are given in Table 1. We use fully connected PNNs with three layers as subnetworks and evaluate the log-determinant exactly by backpropagation.

4.1 Unconditional Examples.

In the following, we apply proximal residual flows for density estimation, i.e., we are in the setting of Section 2.

Toy Densities. First, we train proximal residual flows onto some toy densities, namely 8 modes, two moons, two circles and checkboard. Samples from the training data and the reconstruction with proximal residual flows are given in Figure 1. We observe that the proximal residual flow is able to learn all of the toy densities very well, even though it was shown in [21] that a diffeomorphism, which pushes forward a unimodal distribution to a multimodal one must have a large Lipschitz constant.

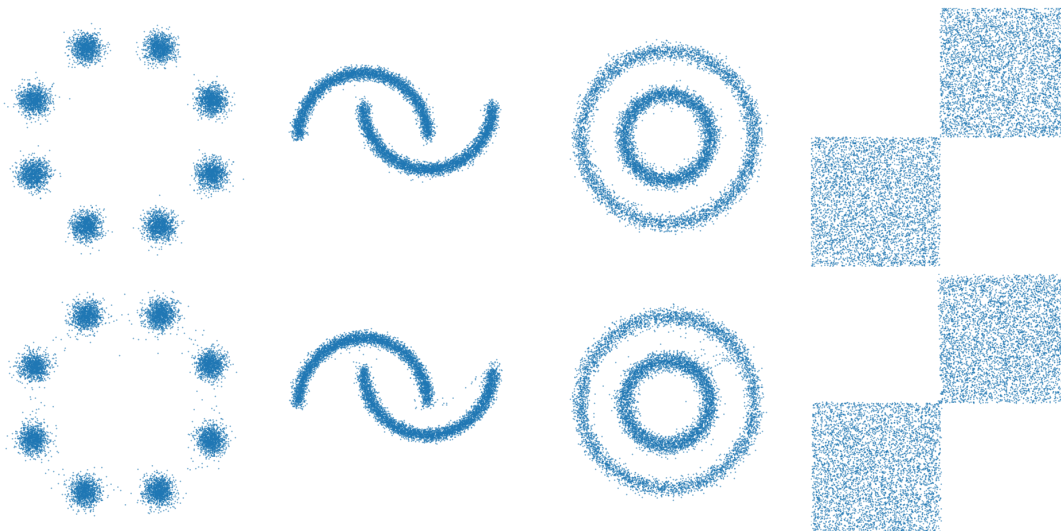


Figure 1: Reconstruction of toy densities. Top: Ground truth, Bottom: Reconstructions with proximal residual flows.

Alanine Dipeptide. Next, we evaluate proximal residual flows for an example from [1, 47]¹. Here, we aim to estimate the density of molecular structures of alanine dipeptide molecules. The structure of such molecules is described by an 66-dimensional vector. For evaluating the quality of the results, we follow [47] and consider the marginal distribution onto the torsion angles, as introduced in [38]. Afterwards, we consider the empirical Kullback Leibler divergence between these marginal distributions of the training data and the reconstruction by the proximal residual flows based on samples. We compare our results with a normalizing flow consisting of 20 real NVP blocks with subnetworks consisting of 3 fully connected layers and a hidden dimension of 128 and a residual flows with 20 residual blocks, where each subnetwork has three hidden layers with 128 neurons. The results are given in Table 2. We observe that the proximal residual flow yields better results than the large real NVP network and the residual flow.

4.2 Posterior Reconstruction

Now, we aim to find a conditional proximal residual flow for reconstructing the posterior distribution $P_{X|Y=y}$ for all $y \in \mathbb{R}^d$. That is, we consider the setting from Section 3.

Circle. First, we consider the inverse problem (2) specified as follows. Let the prior distribution P_X be the convolution of uniform distribution on the unit circle in \mathbb{R}^2 with the

¹For the data generation and evaluation of this example, we use the code of [47] available at https://github.com/noegroup/stochastic_normalizing_flows.

Method	ϕ	γ_1	ψ	γ_2	γ_3
Real NVP	0.12 ± 0.05	0.14 ± 0.04	0.06 ± 0.03	0.04 ± 0.01	0.07 ± 0.01
Residual Flows	0.12 ± 0.11	0.24 ± 0.29	0.10 ± 0.08	0.06 ± 0.03	0.07 ± 0.02
Proximal Residual Flow	0.05 ± 0.02	0.06 ± 0.01	0.03 ± 0.00	0.05 ± 0.01	0.05 ± 0.01

Table 2: Empirical Kullback Leibler divergence between one-dimensional marginal distributions corresponding to the torsion angles ϕ , γ_1 , ψ , γ_2 and γ_3 . The results are averaged over five independent runs.

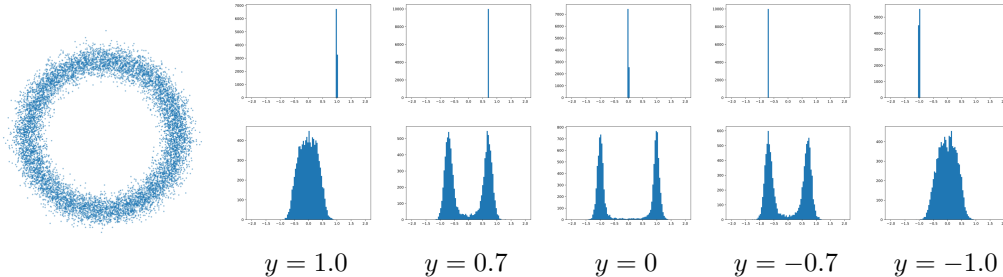


Figure 2: Left: Samples from the prior distribution of X for the circle example. Right: Histograms of samples from the reconstructed posterior distribution $P_{X|Y=y} \approx \mathcal{T}(\cdot, y)_{\#}^{-1} P_Z$ for $y \in \{1, 0.7, 0, -0.7, -1\}$ within the circle example. Top: first coordinate, Bottom: second coordinate.

normal distribution $\epsilon \sim \mathcal{N}(0, 0.1^2 I_2)$. Samples of P_X are illustrated on the left of Figure 2. Further let the operator $F: \mathbb{R}^2 \rightarrow \mathbb{R}$ be given by $y := F(x_1, x_2) = x_1$ and define the noise distribution by $\eta \sim \mathcal{N}(0, 0.02^2 I)$.

Now, we train a conditional proximal residual flow $\mathcal{T}(x, y)$ such that it holds approximately

$$P_{X|Y=y} \approx \mathcal{T}(\cdot, y)_{\#}^{-1} P_Z$$

The right side of Figure 2 shows histograms of samples from the reconstructed posterior distribution $\mathcal{T}(\cdot, y)_{\#}^{-1} P_Z$ for $y \in \{1, 0.7, 0, -0.7, -1\}$. As expected the estimation of $P_{X|Y=y}$ is unimodal for $y \in \{1, -1\}$ and bimodal for $y \in \{0.7, 0, -0.7\}$.

Scatterometry. Next, we apply proximal residual flows to a Bayesian inverse problem in scatterometry with a nonlinear forward operator $F: \mathbb{R}^3 \rightarrow \mathbb{R}^{23}$. It describes the diffraction of monochromatic lights on line gratings which is a non-destructive technique to determine the structures of photo masks. For a detailed description, we refer to [24, 25]. We use the code of [20]² for the data generation, evaluation and the representation of the forward operator.

²available at <https://github.com/PaulLyonel/conditionalSNF>.

	Real NVP	Residual Flows	Proximal Residual Flows
KL	0.773 ± 0.289	0.913 ± 0.407	0.637 ± 0.263

Table 3: Average empirical KL divergence of the different reconstructions for the scatterometry example.

As no prior information about the parameters x is given, we choose the prior distribution P_X to be the uniform distribution on $[-1, 1]^3$. Since we assume for normalizing flows that P_X has a strictly positive density p_X , we relax the probability density function of the uniform distribution for $x = (x_1, x_2, x_3) \in \mathbb{R}^3$ by

$$p_X(x) := q(x_1)q(x_2)q(x_3), \quad q(x) := \begin{cases} \frac{\alpha}{2\alpha+2} \exp(-\alpha(-1-x)), & \text{for } x < -1, \\ \frac{\alpha}{2\alpha+2}, & \text{for } x \in [-1, 1], \\ \frac{\alpha}{2\alpha+2} \exp(-\alpha(x-1)), & \text{for } x > 1, \end{cases}$$

where $\alpha \gg 0$ is some constant. Note that for large α and x_i outside of $[-1, 1]$ the function q becomes small such that p_X is small outside of $[-1, 1]^3$. In our numerical experiments, α is set to $\alpha = 1000$.

We compare the proximal residual flow with the normalizing flow with real NVP architecture from [20] and with a residual flow of 20 residual blocks, where each subnetwork has three hidden layers with 128 neurons. As a quality measure, we use the empirical KL divergence of $P_{X|Y=y}$ and $\mathcal{T}(y, \cdot)_{\#}^{-1} P_Z$ for 100 independent samples with 540000 samples on a $75 \times 75 \times 75$ grid. As a ground truth, we use samples from $P_{X|Y=y}$ which are generated by the Metropolis Hastings algorithm, see [20]. The average empirical KL divergences of the reconstructed posterior distributions over 100 observations are given in Table 3. The proximal residual flow gives the best reconstructions.

Mixture models. Next, we consider the Bayesian inverse problem (2), where the forward operator $F: \mathbb{R}^{50} \rightarrow \mathbb{R}^{50}$ is linear and given by the diagonal matrix $A := 0.1 \text{diag}((\frac{1}{n})_{n=1}^{50})$. Moreover, we add Gaussian noise with standard deviation 0.05. As prior distribution P_X , we choose a Gaussian mixture model with 5 components, where we draw the means uniformly from $[-1, 1]^{50}$ and set the covariances to $0.01^2 I$. Note that in this setting, the posterior distribution can be computed analytically, see [20, Lem. 6.1].

We compare our results with a normalizing flow consisting of 20 real NVP blocks with subnetworks consisting of 3 fully connected layers and a hidden dimension of 128 and a residual flow with 20 residual blocks, where each subnetwork has three hidden layers with 128 neurons. Since the evaluation of the empirical KL divergence is intractable in high dimensions, we use the empirical Wasserstein distance as an error measure. The results are given in Table 4. We observe, that the proximal residual flows outperforms both comparing methods significantly.

	Real NVP	Residual Flows	Proximal Residual Flows
Wasserstein-2 distance	2.122 ± 1.007	1.374 ± 0.050	1.028 ± 0.079

Table 4: Average Wasserstein-2 distance for the reconstructed posteriors to the ground truth over 100 observations.

5 Conclusions

We introduced proximal residual flows, which improve the expressiveness of residual flows by the use of proximal neural networks. In particular, we proved that proximal residual flows are invertible, even though the Lipschitz constant of the subnetworks is larger than one. Afterwards, we extended the framework of proximal residual flows to the problem of posterior reconstruction within Bayesian inverse problems by using conditional generative modelling. Finally, we demonstrated the performance of proximal residual flows by numerical examples.

This work can be extended in several directions. First, it is an open question, how to generalize the training procedure in this paper to convolutional networks. In particular, finding an efficient algorithm which computes the orthogonal projection onto the space of orthogonal convolutions with limited filter length is left for future research. Moreover, every invertible neural network architecture requires an exploding Lipschitz constant for reconstructing multimodal [21, 44] or heavy tailed distributions [32]. To overcome these topological constraints, the authors of [1, 20, 35, 47] propose to combine normalizing flows with stochastic sampling methods. Finally, we could improve the expressiveness of proximal residual flows by combining them with other generative models, see e.g. [19].

Acknowledgements

Funding by the German Research Foundation (DFG) within the project STE 571/15-1 is gratefully acknowledged.

References

- [1] M. Arbel, A. Matthews, and A. Doucet. Annealed flow transport Monte Carlo. In *International Conference on Machine Learning*, pages 318–330. PMLR, 2021.
- [2] L. Ardizzone, J. Kruse, C. Rother, and U. Köthe. Analyzing inverse problems with invertible neural networks. In *International Conference on Learning Representations*, 2018.
- [3] L. Ardizzone, C. Lüth, J. Kruse, C. Rother, and U. Köthe. Guided image generation with conditional invertible neural networks. *arXiv preprint arXiv:1907.02392*, 2019.

- [4] J. Behrmann, W. Grathwohl, R. T. Chen, D. Duvenaud, and J.-H. Jacobsen. Invertible residual networks. In *International Conference on Machine Learning*, pages 573–582, 2019.
- [5] J. Bolte, S. Sabach, and M. Teboulle. Proximal alternating linearized minimization for nonconvex and nonsmooth problems. *Mathematical Programming*, 146(1):459–494, 2014.
- [6] S. Boyd, N. Parikh, E. Chu, B. Peleato, and J. Eckstein. Distributed optimization and statistical learning via the alternating direction method of multipliers. *Foundations and Trends in Machine learning*, 3(1):1–122, 2011.
- [7] R. T. Chen, Y. Rubanova, J. Bettencourt, and D. K. Duvenaud. Neural ordinary differential equations. *Advances in Neural Information Processing Systems*, 31, 2018.
- [8] R. T. Q. Chen, J. Behrmann, D. K. Duvenaud, and J.-H. Jacobsen. Residual flows for invertible generative modeling. In *Advances in Neural Information Processing Systems*, volume 32. Curran Associates, Inc., 2019.
- [9] P. L. Combettes and J.-C. Pesquet. Proximal splitting methods in signal processing. In *Fixed-point algorithms for inverse problems in science and engineering*, pages 185–212. Springer, 2011.
- [10] P. L. Combettes and J.-C. Pesquet. Deep neural network structures solving variational inequalities. *Set-Valued and Variational Analysis*, 28(3):491–518, 2020.
- [11] N. De Cao, I. Titov, and W. Aziz. Block neural autoregressive flow. In *Uncertainty in artificial intelligence*, pages 1263–1273. PMLR, 2020.
- [12] A. Denker, M. Schmidt, J. Leuschner, and P. Maass. Conditional invertible neural networks for medical imaging. *Journal of Imaging*, 7(11):243, 2021.
- [13] L. Dinh, D. Krueger, and Y. Bengio. NICE: non-linear independent components estimation. In Y. Bengio and Y. LeCun, editors, *3rd International Conference on Learning Representations, Workshop Track Proceedings*, 2015.
- [14] L. Dinh, J. Sohl-Dickstein, and S. Bengio. Density estimation using real NVP. In *International Conference on Learning Representations*, 2017.
- [15] C. Durkan, A. Bekasov, I. Murray, and G. Papamakarios. Neural spline flows. *Advances in Neural Information Processing Systems*, 2019.
- [16] R. Glowinski, S. J. Osher, and W. Yin. *Splitting methods in communication, imaging, science, and engineering*. Springer, 2017.

- [17] H. Gouk, E. Frank, B. Pfahringer, and M. J. Cree. Regularisation of neural networks by enforcing Lipschitz continuity. *Machine Learning*, 110(2):393–416, 2021.
- [18] W. Grathwohl, R. T. Chen, J. Bettencourt, I. Sutskever, and D. Duvenaud. FFJORD: Free-form continuous dynamics for scalable reversible generative models. In *International Conference on Learning Representations*, 2018.
- [19] P. Hagemann, J. Hertrich, and G. Steidl. Generalized normalizing flows via Markov Chains. *arXiv preprint arXiv:2111.12506*, 2021.
- [20] P. Hagemann, J. Hertrich, and G. Steidl. Stochastic normalizing flows for inverse problems: a Markov Chains viewpoint. *SIAM/ASA Journal on Uncertainty Quantification*, 10(3):1162–1190, 2022.
- [21] P. Hagemann and S. Neumayer. Stabilizing invertible neural networks using mixture models. *Inverse Problems*, 37(8):085002, 2021.
- [22] M. Hasannasab, J. Hertrich, S. Neumayer, G. Plonka, S. Setzer, and G. Steidl. Parseval proximal neural networks. *Journal of Fourier Analysis Applications*, 26:59, 2020.
- [23] K. He, X. Zhang, S. Ren, and J. Sun. Deep residual learning for image recognition. In *Proceedings of the IEEE Conference on Computer Vision and Pattern Recognition*, pages 770–778, 2016.
- [24] S. Heidenreich, H. Gross, and M. Bär. Bayesian approach to the statistical inverse problem of scatterometry: Comparison of three surrogate models. *International Journal for Uncertainty Quantification*, 5(6), 2015.
- [25] S. Heidenreich, H. Gross, and M. Bär. Bayesian approach to determine critical dimensions from scatterometric measurements. *Metrologia*, 55(6):S201, Dec. 2018.
- [26] J. Hertrich, S. Neumayer, and G. Steidl. Convolutional proximal neural networks and plug-and-play algorithms. *Linear Algebra and its Applications*, 631:203–234, 2021.
- [27] J. Hertrich and G. Steidl. Inertial stochastic PALM and applications in machine learning. *Sampling Theory, Signal Processing, and Data Analysis*, 20(4), 2022.
- [28] N. J. Higham. *Functions of Matrices: Theory and Computation*. SIAM, Philadelphia, 2008.
- [29] R. A. Horn and C. R. Johnson. *Matrix Analysis*. Oxford University Press, 2013.
- [30] C.-W. Huang, R. T. Chen, C. Tsirigotis, and A. Courville. Convex potential flows: Universal probability distributions with optimal transport and convex optimization. In *International Conference on Learning Representations*, 2020.

- [31] C.-W. Huang, D. Krueger, A. Lacoste, and A. Courville. Neural autoregressive flows. In *International Conference on Machine Learning*, pages 2078–2087, 2018.
- [32] P. Jaini, I. Kobyzev, Y. Yu, and M. Brubaker. Tails of Lipschitz triangular flows. In *International Conference on Machine Learning*, pages 4673–4681. PMLR, 2020.
- [33] D. P. Kingma and J. Ba. Adam: A method for stochastic optimization. In *International Conference on Learning Representations*, 2015.
- [34] D. P. Kingma and P. Dhariwal. Glow: Generative flow with invertible 1x1 convolutions. *Advances in neural information processing systems*, 31, 2018.
- [35] A. G. Matthews, M. Arbel, D. J. Rezende, and A. Doucet. Continual repeated annealed flow transport Monte Carlo. *arXiv preprint arXiv:2201.13117*, 2022.
- [36] M. Mirza and S. Osindero. Conditional generative adversarial nets. *arXiv preprint arXiv:1411.1784*, 2014.
- [37] T. Miyato, T. Kataoka, M. Koyama, and Y. Yoshida. Spectral normalization for generative adversarial networks. In *International Conference on Learning Representations*, 2018.
- [38] F. Noé, S. Olsson, J. Köhler, and H. Wu. Boltzmann generators: Sampling equilibrium states of many-body systems with deep learning. *Science*, 365(6457):eaaw1147, 2019.
- [39] D. Onken, S. W. Fung, X. Li, and L. Ruthotto. OT-flow: Fast and accurate continuous normalizing flows via optimal transport. In *Proceedings of the AAAI Conference on Artificial Intelligence*, volume 35, pages 9223–9232, 2021.
- [40] G. Papamakarios, T. Pavlakou, , and I. Murray. Masked autoregressive flow for density estimation. *Advances in Neural Information Processing Systems*, page 2338–2347, 2017.
- [41] J.-C. Pesquet, A. Repetti, M. Terris, and Y. Wiaux. Learning maximally monotone operators for image recovery. *SIAM Journal on Imaging Sciences*, 14(3):1206–1237, 2021.
- [42] T. Pock and S. Sabach. Inertial proximal alternating linearized minimization (iPALM) for nonconvex and nonsmooth problems. *SIAM Journal on Imaging Sciences*, 9(4):1756–1787, 2016.
- [43] D. Rezende and S. Mohamed. Variational inference with normalizing flows. In *International Conference on Machine Learning*, pages 1530–1538. PMLR, 2015.
- [44] A. Salmona, V. De Bortoli, J. Delon, and A. Desolneux. Can push-forward generative models fit multimodal distributions? In *Advances in Neural Information Processing Systems*, 2022.

- [45] H. Sedghi, V. Gupta, and P. M. Long. The singular values of convolutional layers. In *International Conference on Learning Representations*, 2018.
- [46] K. Sohn, H. Lee, and X. Yan. Learning structured output representation using deep conditional generative models. *Advances in Neural Information Processing Systems*, 28, 2015.
- [47] H. Wu, J. Köhler, and F. Noé. Stochastic normalizing flows. *Advances in Neural Information Processing Systems*, 33:5933–5944, 2020.